Attitude Determination and Control System Design of the Hubble Space Telescope

Marco Hinojosa

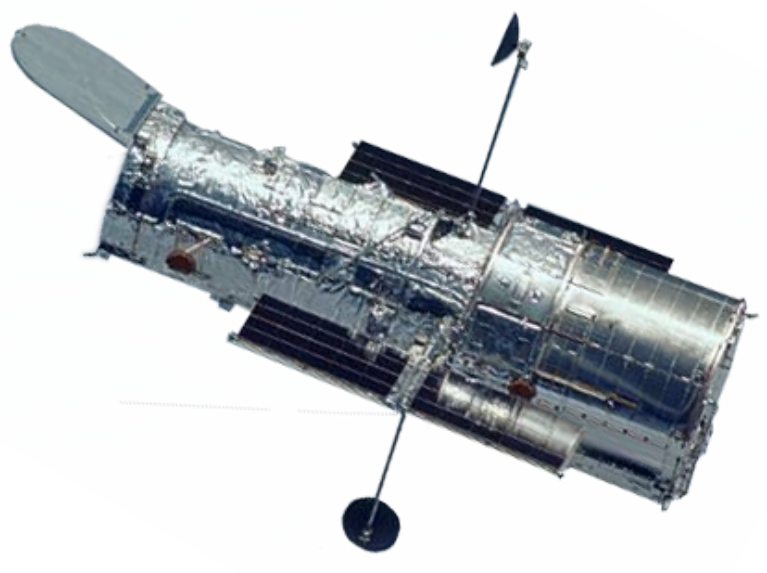

AA 279C - Spacecraft Attitude Determination and Control
Stanford University

GitHub: `https://github.com/marco-hinojosa/HST-ADCS`

Revision History

Table 1: Summary of Project Revisions.

Rev	**Changes**
PS1	- Created document - Added problem set 1 material
PS2	- Added problem set 2 material - Added rotation from body to principal axes
PS3	- Added problem set 3 material
PS4	- Added problem set 4 material - Added pointing error for quaternion dynamics - Updated MEKF to correctly track estimates
PS5	- Added problem set 5 material
Extra Stuff	- Added Trajectory Optimization Section - Reorder sections for cohesion - Added computation time to Attitude Estimation

Contents

1 Abstract

This report details the analysis of the attitude determination and control system (ADCS) design for the Hubble Space Telescope. This endeavor encompasses an understanding of the HST's mission objectives and target orbit, as well as the sensors and actuators present on the spacecraft and how they fulfill the requirements for the ADCS system. The report starts with simulations of orbit and attitude trajectories of the HST with and without perturbations. Attitude regulators and LQR trackers for large-angle maneuvers are implemented using MATLAB. Methods for static attitude estimation are discussed and compared to the results of a Multiplicative Extended Kalman Filter based on known hardware specifications of the satellite. Finally, the eigen-axis slew is used as a basis for large-angle trajectory optimization subject to known actuator constraints.

2 Mission Description and Requirements

The Hubble Space Telescope was designed as a direct solution to the problem of image distortion caused by the Earth's atmosphere. Since its launch in 1990, the HST has been fulfilling its mission of enabling astronomers to make extremely high resolution observations of deep space with considerably lower background light than ground-based telescopes. The Space Telescope Science Institute (STScI) at John Hopkins University has served as the science operations center for the HST, while Goddard Space Flight Center has been the control center for the spacecraft. The HST was built by NASA with contributions from the European Space Agency and has undergone five servicing missions since its initial launch. As of today, it has made over one million observations, some of which are the most detailed visible light images ever taken. The future of the HST's ongoing mission is largely dependent upon the extension of the telescope's service contract with NASA. If it is not reboosted, Hubble will undergo a natural atmospheric reentry at some time between 2028 and 2040.

The HST is an inertial-pointing satellite capable of taking images of distant, faint objects from low Earth orbit (LEO). Hubble has an altitude of approximately 540 kilometers and an inclination of 28.5^o that gives the spacecraft a period of approximately 95.5 minutes. The telescope is able to lock onto targets with an error no more than 7/1000th of an arcsecond and has a slew rate of approximately 6^o per minute [2]. To achieve this, Hubble must use three fine guidance sensors (FGSs) to receive highly accurate measurements of its attitude and then control it using four reaction wheels [3]. Hubble also possesses gyroscopes, coarse sun sensors, magnetometers, and fixed head star trackers to determine its attitude to varying degrees of accuracy [5].

3 Spacecraft Model

A 3D CAD model of the Hubble Space Telescope was produced in SolidWorks, using known mass values and dimensions of the spacecraft [1]. This model was then used to determine the values in the Mass Properties table, assuming uniform density. The origin of the HST's body system was arbitrarily designated as the centroid of the bottom circular surface, according to the following figure. A simplified CAD model in which the satellite geometries were represented as boxes was used to determine centroids, normal vectors, and areas of each surface. This is a conservative approximation and simplifies calculations by reducing the total number of values to compute. Conveniently, these numbers are automatically computed in SolidWorks and are tabulated according to normal vector in Area Properties.

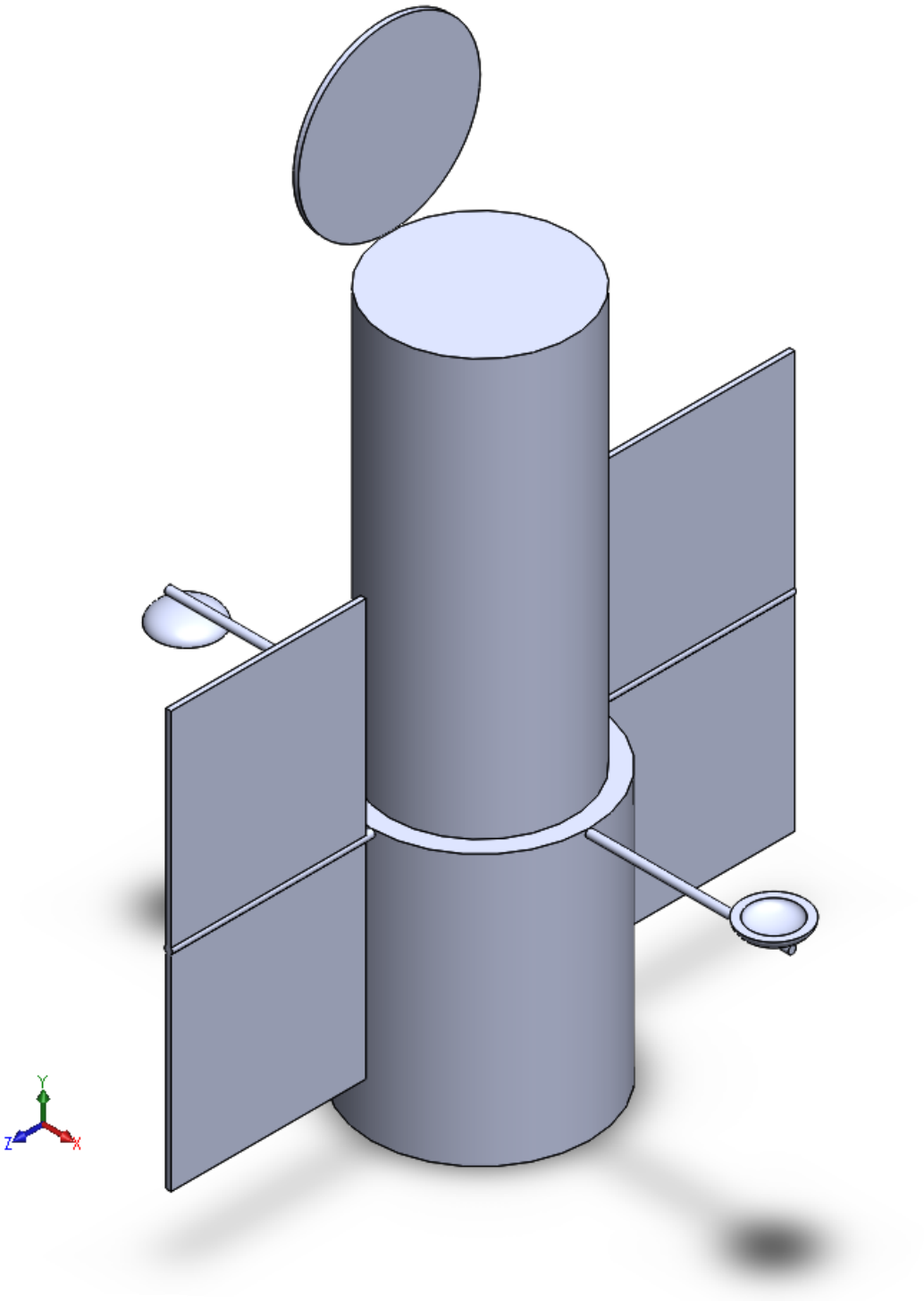

Figure 1: 3D CAD model of Hubble Space Telescope.

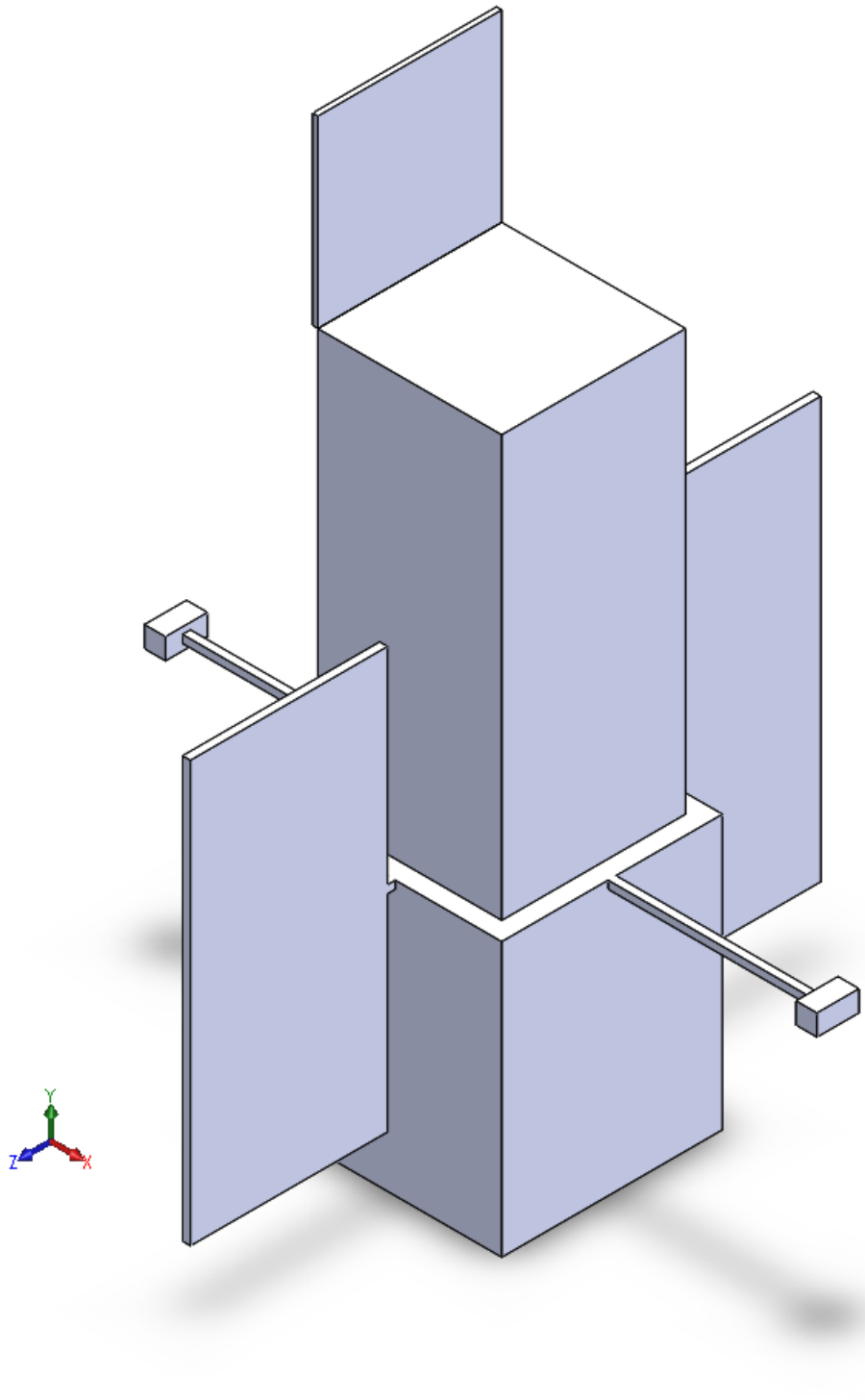

Figure 2: Simplified 3D CAD model of Hubble Space Telescope.

Mass Properties	
Mass (kg)	11,100
Volume (m^3)	156.43
Center of Mass (m) (w.r.t. Origin)	x = -0.01 y = 6.03 z = 0.00
Principal Axes of Inertia (Rotation Matrix from Body to Principal)	I_x = (-0.01, 0.00, -1.00) I_y = (-1.00, 0.00, 0.01) I_z = (0.00, 1.00, 0.00)
Principal Moments of Inertia (kg-m^2) (w.r.t. Center of Mass)	J_{11} = 28525.53 J_{22} = 174815.86 J_{33} = 181630.81
Body-Frame Inertia Matrix (kg-m^2)	${}^B\mathrm{J} = \begin{bmatrix} 181623.33 & -1070.20 & 0.00 \\ -1070.20 & 28533.02 & 0.00 \\ 0.00 & 0.00 & 174815.86 \end{bmatrix}$

Area Properties		
Normal Vector	Centroid (m) w.r.t. Origin	Area (m^2)
$\underline{n}$ = [1, 0, 0]	(x,y,z) = (0.64, 6.59, 0.00)	122.73
$\underline{n}$ = [-1, 0 ,0]	(x,y,z) = (-1.00, 6.59, 0.00)	122.73
$\underline{n}$ = [0, 1, 0]	(x,y,z) = (-0.03, 10.28, 0.00)	20.97
$\underline{n}$ = [0, -1, 0]	(x,y,z) = (-0.03, 0.72, 0.00)	20.97
$\underline{n}$ = [0, 0, 1]	(x,y,z) = (-0.01, 6.28, 1.85)	54.04
$\underline{n}$ = [0, 0, -1]	(x,y,z) = (-0.01, 6.28, -1.85)	54.04

From the tabulated information, the rotation matrix from body axes to principal axes is found to be

$$ {}^B R^P = \begin{bmatrix} I_x \\ I_y \\ I_z \end{bmatrix} = \begin{bmatrix} -0.01 & 0.00 & -1.00 \\ -1.00 & 0.00 & 0.01 \\ 0.00 & 1.00 & 0.00 \end{bmatrix} $$

4 Dynamics

4.1 Orbit Dynamics

4.1.1 Keplerian Initial Conditions

The initial conditions of the simulation are provided as a set of Keplerian orbital elements and an initial epoch date and time. Orbital elements are available for this mission for several epoch times and can be used to replace the initial launch time.

All orbital elements are taken from Wikipedia.org at Epoch: 26 December 2017, 13:18:33 UTC [6].

$a = 6917.5$ km
$e = 0.000287$

$i = 28.47°$
$\Omega = 176.23°$
$\omega = 82.61°$
$M_0 = 319.41°$

4.1.2 Initial Position and Velocity in Inertial Frame

In order to numerically integrate our orbit equation, the initial Keplerian orbital elements must be converted to initial position and velocity vectors in an Earth-Centered Inertial (ECI) frame. Doing so gives the following vectors for the corresponding initial position and velocity in the appropriate ECI frame:

$r_0{}^{ECI} = [\,-5396.0,\ -3721.2,\ 2206.0\,]^T$ [km]
$v_0{}^{ECI} = [\,4.7443,\ -5.2827,\ 2.6893\,]^T$ [km/s]

4.1.3 Unperturbed Orbit

For an unperturbed system, vehicle dynamics behave according to the two-body problem, a simple second-order non-linear ODE expressed as

$$\ddot{\mathbf{r}} + \frac{\mu \mathbf{r}}{r^3} = \mathbf{0}$$

This ODE represents the gravitational acceleration acting upon the vehicle under ideal conditions (notably, the absence of other forces). Using the initial inertial states as provided in the previous section, the equation can be numerically integrated [7]. Neglecting all perturbation forces and gravitational forces from other bodies, the following orbit was integrated over a time spanning 3 complete orbits with a time step of 1 second. Without environmental disturbances, the orbit remains unchanged.

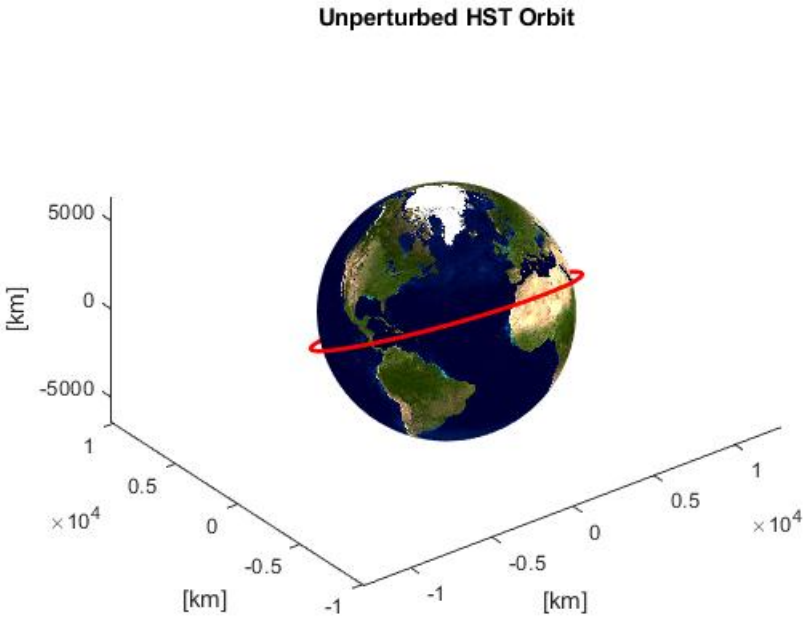

Figure 3: Unperturbed HST Orbit

4.2 Attitude Dynamics

The Gyrostat equation, a modified version of Euler's equation, must be implemented to examine the spin stability of the Hubble Space Telescope,

$$J\dot{\omega} + \dot{\rho} + \omega \times (J\omega + \rho) = \tau = 0$$

where J is the approximate inertia tensor from the simplified CAD model, ω is the angular velocity vector, and ρ is the rotor momentum for a gyrostat. The nominal spin of the HST can be visualized by setting $\rho = 0$ and simulating the dynamics in MATLAB. The equilibrium points and nutation trajectories for various initial velocities are plotted on a momentum sphere in the following figure. All trajectories are subject to the constraint $\|J\omega\| = \|h\| = constant$.

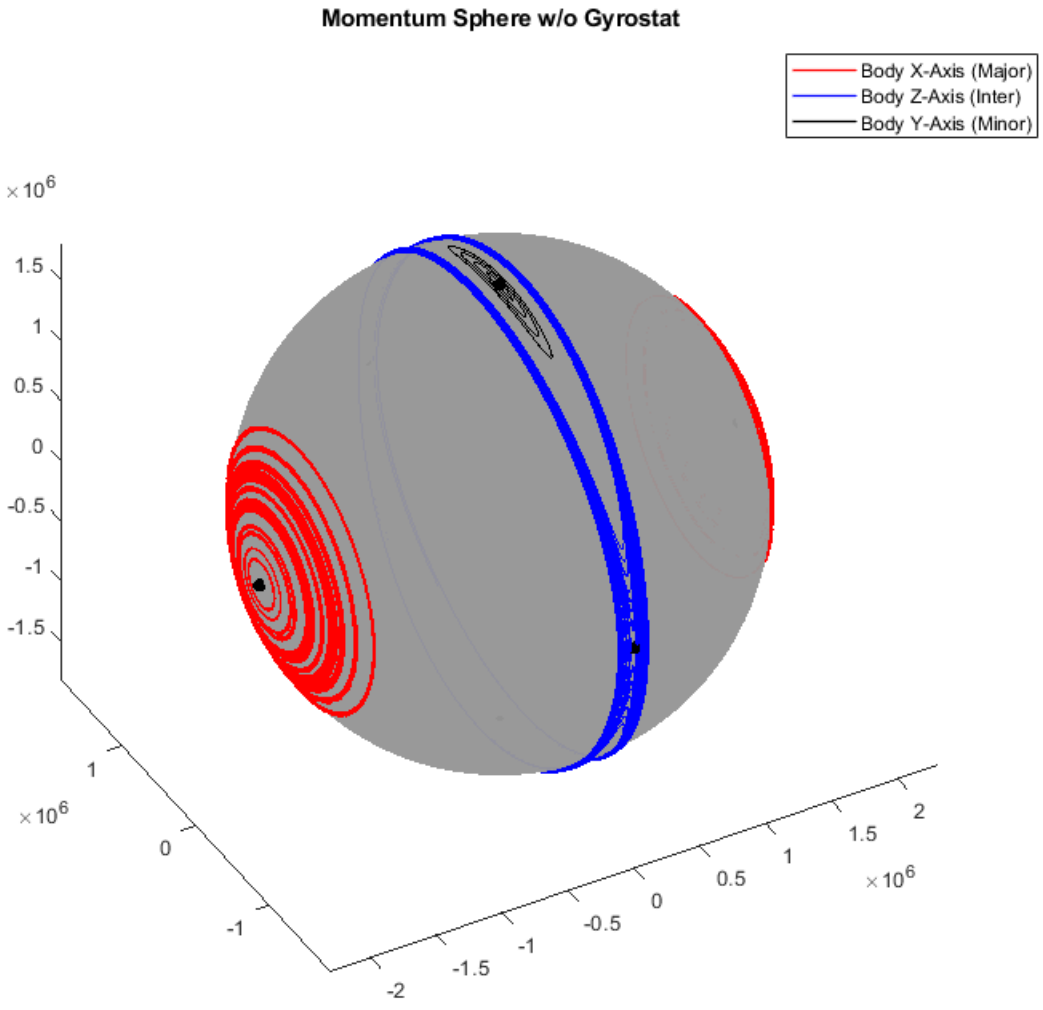

Figure 4: HST Momentum Sphere with Near-Nominal Spin

4.2.1 Passive Stability and Safe Mode

To implement a "safe mode" into the satellite design, we must use superspin and dynamic balance to stabilize the HST about a non-major axis. Based on the uniform-mass assumption of the CAD model created, the major axis corresponds to the x-axis in the body frame (rotation about this axis is a flat spin). For the sake of designing a safe mode, the body y-axis was arbitrarily selected to be the inertially fixed direction. To obtain the dynamic balance condition, the satellite and rotor must be in equilibrium, ${}^B\dot{\omega} = \dot{\rho} = 0$. For a nominal spin about this "effective major axis", the necessary rotor momentum can be computed from the equation

$$\rho = (J_{\text{eff}} - J_{33})\|\omega\|$$

where $J_{\text{eff}} = 1.2J_{33}$ for a conservative margin. Because we are assuming that there are zero external torques on the system, it is also safe to assume that $\dot{\rho} = 0$. Inserting these new values into the Gyrostat equation with small perturbations in the initial conditions results in the following nutation about the body y-axis. Visibly, the satellite is more tolerant of perturbations without moving into an unstable spin.

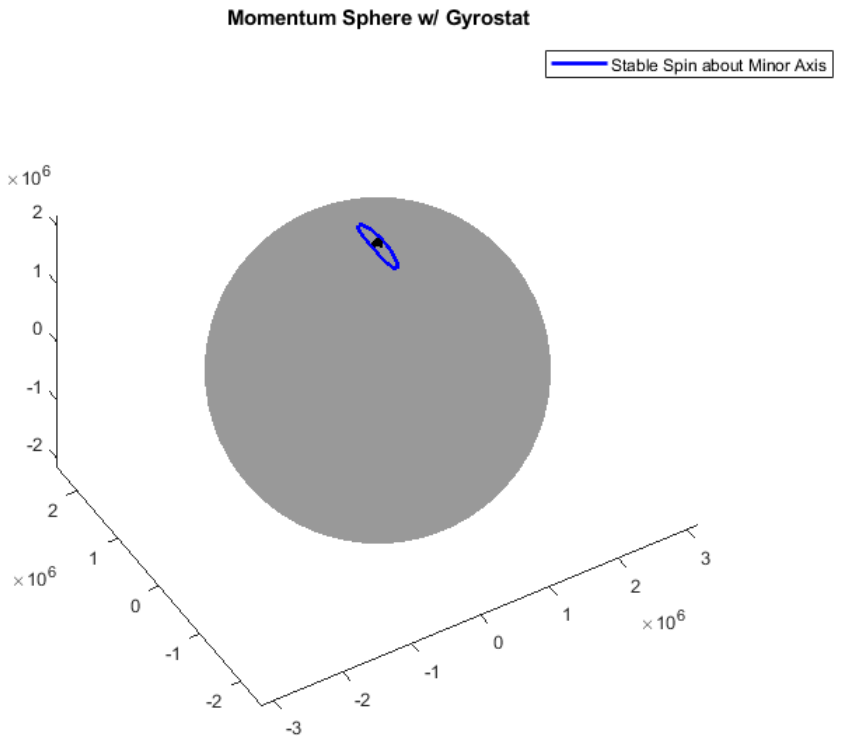

Figure 5: HST Superspin about Non-Major Axis

4.2.2 Unperturbed Quaternion Dynamics

Simulating the gyrostat dynamics along with the orbit propagation is a simple matter of augmenting the existing state vector to include angular velocity, attitude quaternion, and rotor momentum and including

the dynamics of each state element into our ODE solver. For the "safe mode" conditions, the components of the attitude quaternion of the HST are simulated and plotted over fifteen seconds. The simulated results show nutation with both the quaternion and angular velocity.

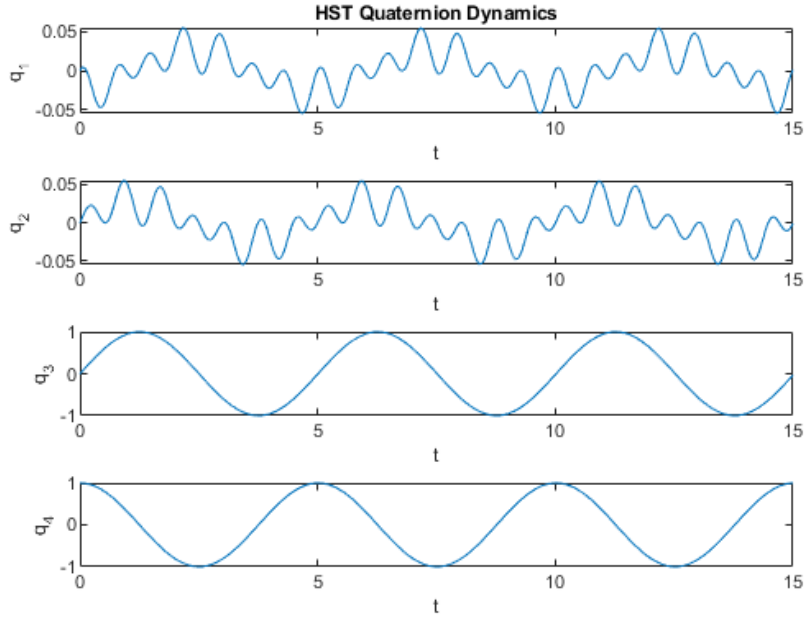

Figure 6: HST Quaternion

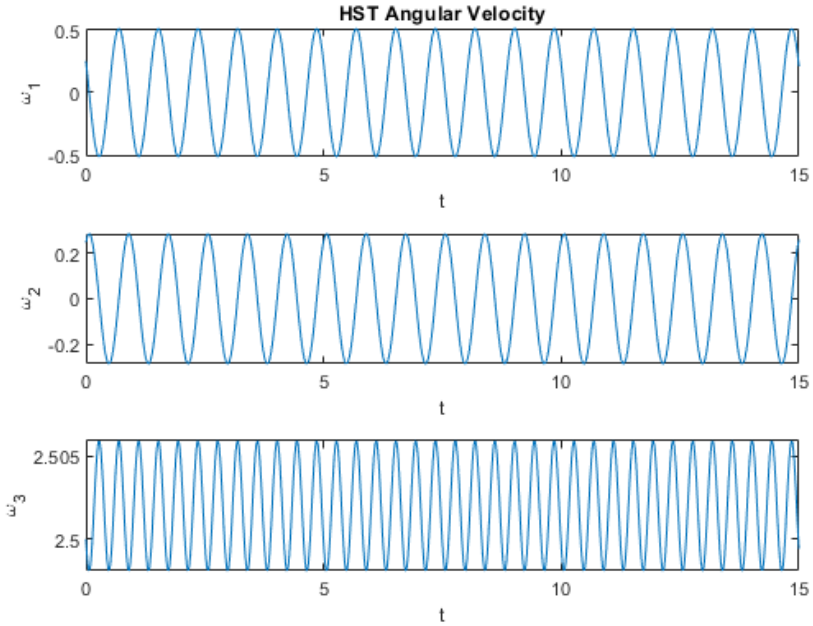

Figure 7: HST Angular Velocity

4.3 Perturbed Dynamics

4.3.1 Environmental Torques

The relevant environmental effects of the HST's low Earth orbit are gravity gradient torque and atmospheric drag. The equation for gravity gradient torque in the inertial frame is

$$\tau_g = \frac{3\mu}{({r_0}^T r_0)^{5/2}} r_0 \times J r_0$$

where r_0 is the position vector of the spacecraft from the Earth in ECI coordinates and J is the inertial-frame spacecraft inertia. The equation for atmospheric drag force and drag torque are

$$\begin{aligned} {F_D}^i &= \frac{1}{2}\rho C_D \|v_{rel}\| v_{rel} S^i \max(\cos(\theta^i), 0) \\ \tau_D &= \sum r^i \times {F_D}^i \end{aligned}$$

where $C_D = 2.2$, $v_{rel} = v_{ECI} + \Omega_E \times r_{ECI}$, S^i is the reference area of the drag surfaces, and θ^i is the angle of incidence between the velocity vector and each plate.

Starting at rest, these effects can be simulated over a full day (or about 15 orbits) to achieve the results shown in the following figures. As expected, the effects of atmospheric drag on the orbit over one day are almost imperceptible on a trajectory plot, but a small orbital decay can be observed when plotted versus time. Similarly, the angular velocity and quaternion dynamics have a periodic component as the satellite orbits as well as a secular drift due to the environmental torques.

- Max Aerodynamic Torque = 0.0106 N-m
- Max Gravity Gradient Torque = 6.3174 $\times 10^{-4}$ N-m
- The mean magnitude of both torques over a full day is 0.0049 N-m. The maximum accumulated change in angular momentum over a full day is 58.03 kg-m^2/s = 58.03 N-m-s.
- Although the environmental effects are small, over long periods of time they have a substantial effect on the attitude stability of the HST. Fortunately, a comparison of max angular momentum and max torque indicate that the control systems on-board the satellite are more than capable of negating these effects. Assuming the angular momentum is equally distributed between each of the HST's four reaction wheels, it would take about twenty-four days for them to saturate and require momentum dumping.

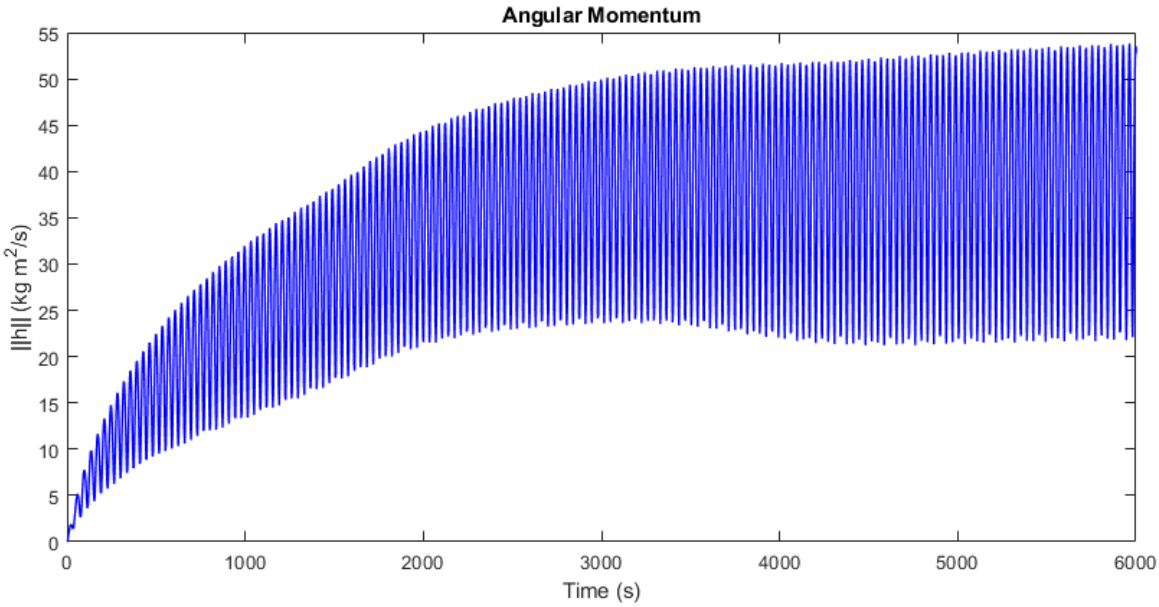

Figure 8: Perturbed Angular Momentum.

4.4 HST Attitude Control System

4.4.1 Actuator Specifications

The HST has reaction wheels and magnetorquers in its Pointing Control System (PCS). To determine the actuator Jacobians required to simulate controlled attitude dynamics, one must first express the torques as linear equations. The equation for reaction wheel torque is

$$
\begin{aligned}
{}^{B}\tau_w &= \sum \dot{\omega}_i = \sum {}^{B}a_i \|\dot{\omega}\|_i \\
&= \begin{bmatrix} {}^{B}a_1 & {}^{B}a_2 & {}^{B}a_3 & {}^{B}a_4 \end{bmatrix} \begin{bmatrix} \|\dot{\omega}\|_1 \\ \|\dot{\omega}\|_2 \\ \|\dot{\omega}\|_3 \\ \|\dot{\omega}\|_4 \end{bmatrix} = {}^{B}B_w u_w
\end{aligned}
$$

where ${}^{B}a_i$ is the normal unit vector for each reaction wheel. The equation for coil torque is

$$
\begin{aligned}
{}^{B}\tau_c &= \sum m_{ci} \times {}^{B}B = \sum -{}^{B}B \times m_{ci} = \sum (-{}^{B}B \times {}^{B}a_i)\|m_c\|_i \\
&= \begin{bmatrix} -{}^{B}B \times {}^{B}a_1 & -{}^{B}B \times {}^{B}a_2 & -{}^{B}B \times {}^{B}a_3 & -{}^{B}B \times {}^{B}a_4 \end{bmatrix} \begin{bmatrix} \|m_c\|_1 \\ \|m_c\|_2 \\ \|m_c\|_3 \\ \|m_c\|_4 \end{bmatrix} = {}^{B}B_c u_c
\end{aligned}
$$

where B is the Earth's magnetic field vector, ${}^{B}a_i$ are the dipole moment unit vectors, and $\|m_c\|_i$ are the dipole moment strengths.

- Reaction Wheel Assemblies (RWAs): Hubble utilizes four variable-rate, fixed-spin-axis reaction wheels to produce torques to rotate the spacecraft. The RWAs are arranged in a canted-pyramidal

configuration with each spin axis pointing in a different direction such that they can be used in a variety of combinations for pointing. Each reaction wheel is approximately two feet wide, and at their fastest speed they can rotate the HST a full 360^o in about one hour.

- Max Torque: 0.82 N-m (per wheel)
- Max Angular Momentum: 350 N-m-s at 3200 RPM (per wheel)
- Actuator Position Vectors (Body Frame, based on Simplified CAD Model):
  - RWA1: [1.75, 6.00, 1.75]
  - RWA2: [-1.75, 6.00, 1.75]
  - RWA3: [-1.75, 6.00, -1.75]
  - RWA4: [1.75, 6.00, -1.75]
- Actuator Orientation Unit Vectors (Body Frame, based on Simplified CAD Model):
  - RWA1: ${}^B a_1 = \left[-\frac{1}{\sqrt{3}}, \frac{1}{\sqrt{3}}, -\frac{1}{\sqrt{3}}\right]^T$
  - RWA2: ${}^B a_2 = \left[\frac{1}{\sqrt{3}}, \frac{1}{\sqrt{3}}, -\frac{1}{\sqrt{3}}\right]^T$
  - RWA3: ${}^B a_3 = \left[\frac{1}{\sqrt{3}}, \frac{1}{\sqrt{3}}, \frac{1}{\sqrt{3}}\right]^T$
  - RWA4: ${}^B a_4 = \left[-\frac{1}{\sqrt{3}}, \frac{1}{\sqrt{3}}, \frac{1}{\sqrt{3}}\right]^T$
- Actuator Jacobian: ${}^B B_c = \begin{bmatrix} {}^B a_1 & {}^B a_2 & {}^B a_3 & {}^B a_4 \end{bmatrix} = \begin{bmatrix} -\frac{1}{\sqrt{3}} & \frac{1}{\sqrt{3}} & \frac{1}{\sqrt{3}} & -\frac{1}{\sqrt{3}} \\ \frac{1}{\sqrt{3}} & \frac{1}{\sqrt{3}} & \frac{1}{\sqrt{3}} & \frac{1}{\sqrt{3}} \\ -\frac{1}{\sqrt{3}} & -\frac{1}{\sqrt{3}} & \frac{1}{\sqrt{3}} & \frac{1}{\sqrt{3}} \end{bmatrix}$

- Magnetorquers: The HST magnetorquers are eight-food iron rods wrapped in wire that produce a magnetic field to either push or pull toward the Earth's magnetic field to rotate the spacecraft or dump reaction wheel momentum. There are four magnetorquers installed on the HST, located at 90^o intervals on the outside of the spacecraft.
  - Max Torque: 0.34 N-m
  - Actuator Position Vector (Body Frame):
    - RWA1: [1.75, 6.00, 0.00]
    - RWA2: [0.00, 6.00, 1.75]
    - RWA3: [-1.75, 6.00, 0.00]
    - RWA4: [0.00, 6.00, -1.75]
  - Actuator Orientation Unit Vector (Body Frame):
    - RWA1: $\left[0, \frac{\sqrt{2}}{2}, \frac{\sqrt{2}}{2}\right]$
    - RWA2: $\left[-\frac{\sqrt{2}}{2}, \frac{\sqrt{2}}{2}, 0\right]$
    - RWA3: $\left[0, \frac{\sqrt{2}}{2}, -\frac{\sqrt{2}}{2}\right]$
    - RWA4: $\left[\frac{\sqrt{2}}{2}, \frac{\sqrt{2}}{2}, 0\right]$
  - Actuator Jacobian: $B_m = \begin{bmatrix} -{}^B B \times {}^B a_1 & -{}^B B \times {}^B a_2 & -{}^B B \times {}^B a_3 & -{}^B B \times {}^B a_4 \end{bmatrix}$

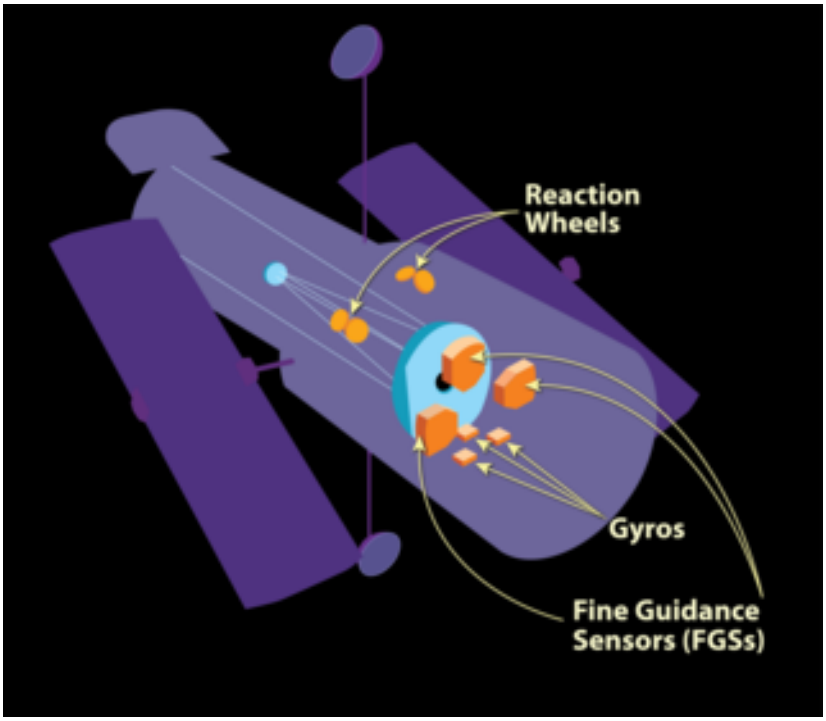

Figure 9: HST Section Cutaway.

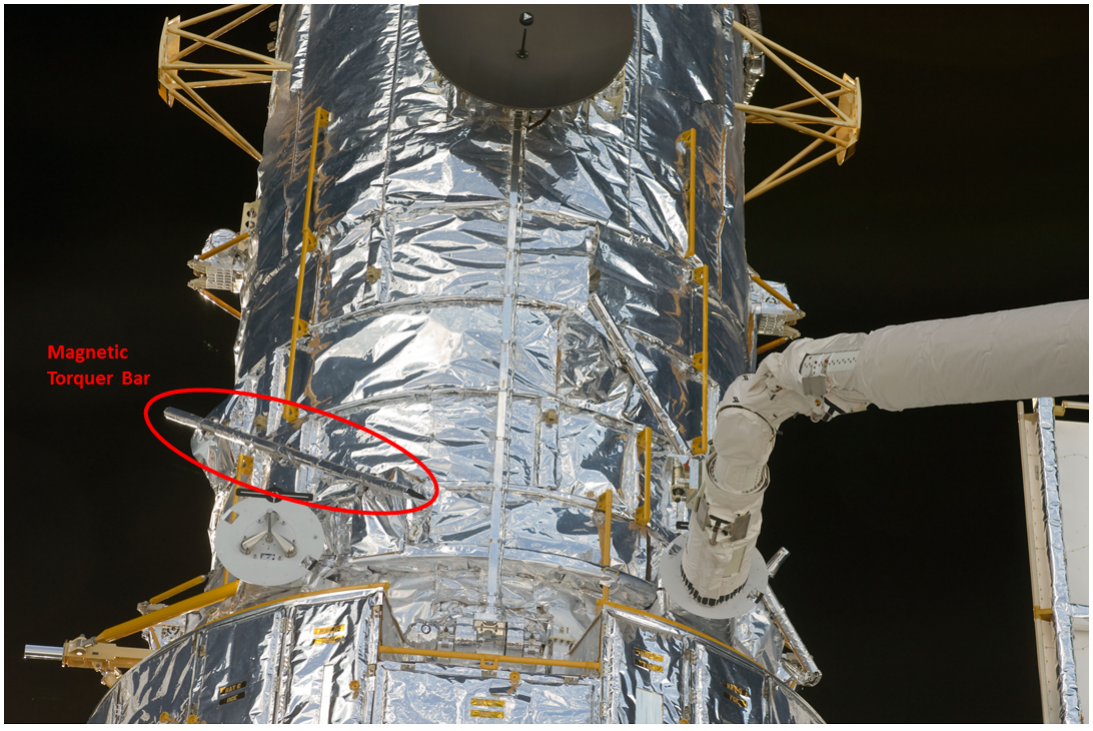

Figure 10: HST Magnetorquer.

4.4.2 Attitude Regulation

For small angle errors, the attitude dynamics of the HST can be linearized such that a linear quadratic regulator can be used to maintain a specified attitude. The results of the controller integrated with the state estimate of the MEKF (discussed in the following section) and the environmental disturbances are shown in the following figures with their respective root-mean-squared errors for various initial errors up to 90^o. In each case, the LQR controller successfully regulates the attitude error over the span of several orbits. The settling characteristics of the attitude dynamics are largely dependent on the Q and R weighting matrices selected for computing the LQR gains, and can be further tuned to improve steady-state performance.

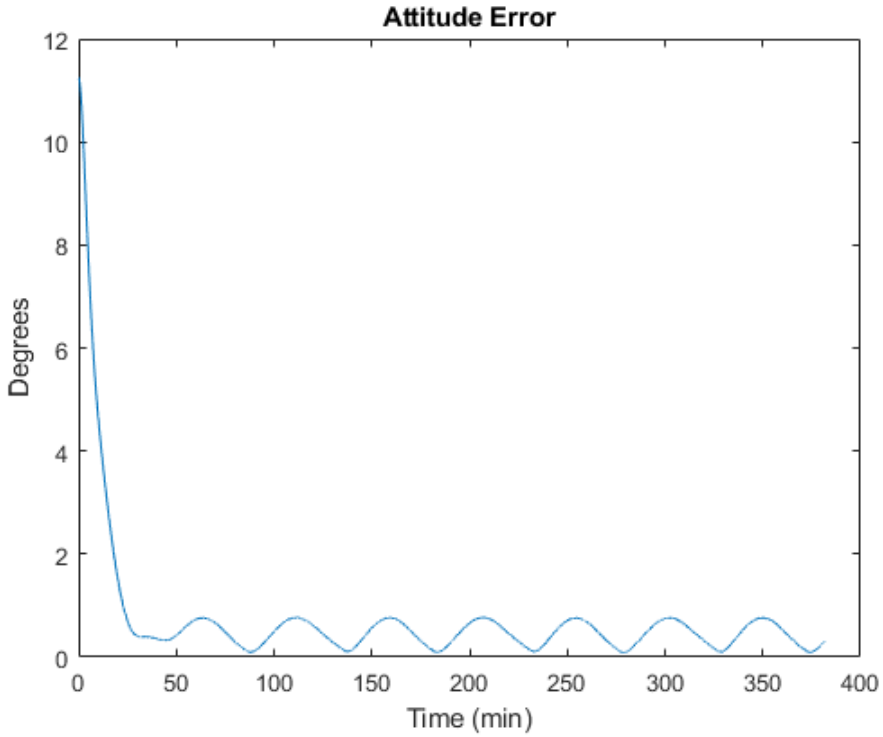

Figure 11: RMS Error: 0.82 degrees.

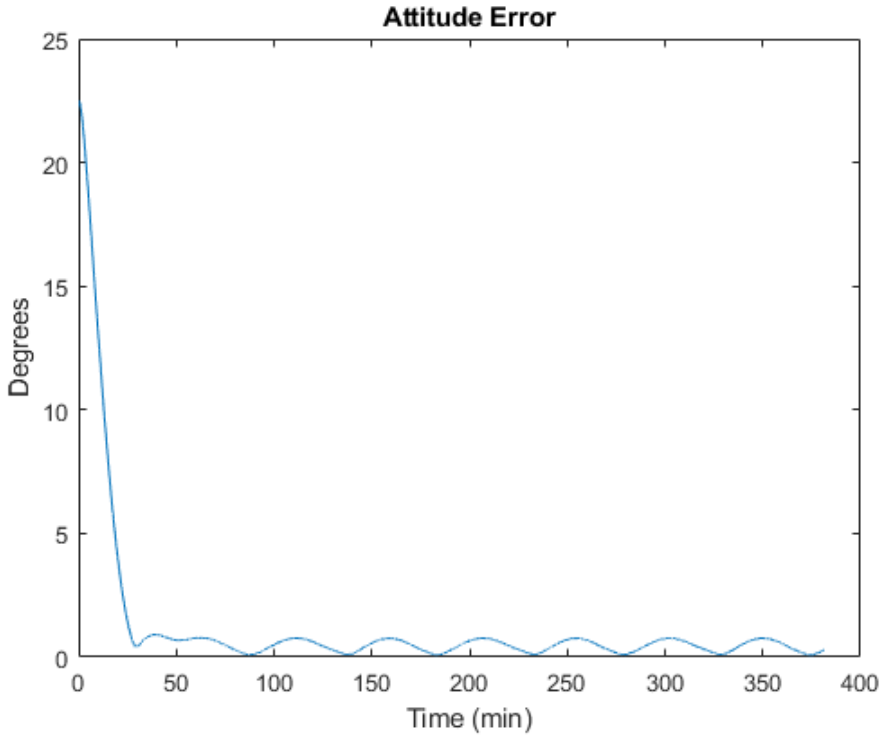

Figure 12: RMS Error: 1.50 degrees.

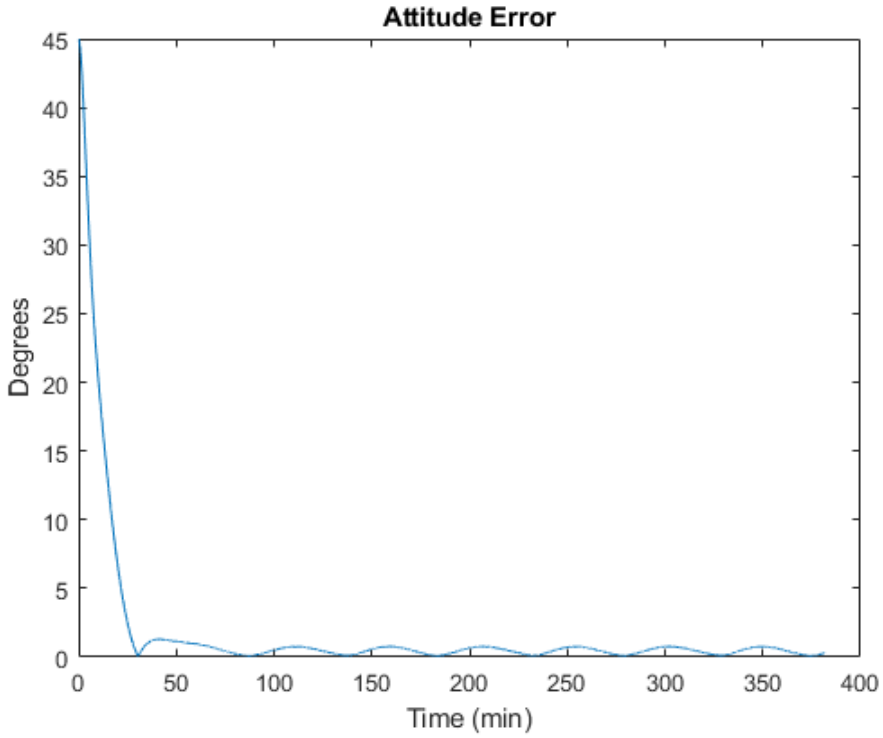

Figure 13: RMS Error: 2.67 degrees.

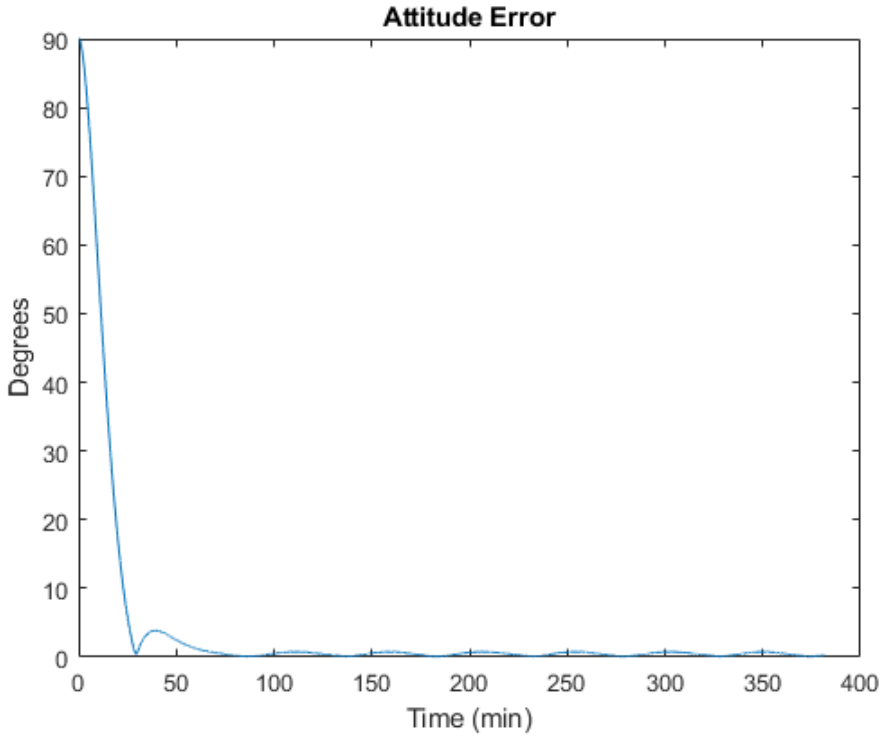

Figure 14: RMS Error: 6.5 degrees.

4.4.3 Eigen-Axis Slew

Using the versine function, a nominal eigen-axis slew maneuver can be designed between initial and final attitudes in a specific maneuver time, which can be used to determine actuator torques with inverse dynamics. The nominal trajectory can be tracked using a linear feedback controller as in the case of attitude regulation. The following figures illustrate the results of an LQR controller used to track a 170^o slew with a 5^o initial error. The nominal maneuver was computed using fourth-order Runge-Kutta integration. Finer tuning of the Q and R matrices is still required in order to achieve better tracking, but the feedback control law improves the performance slightly over open-loop control in the presence of environmental disturbances.

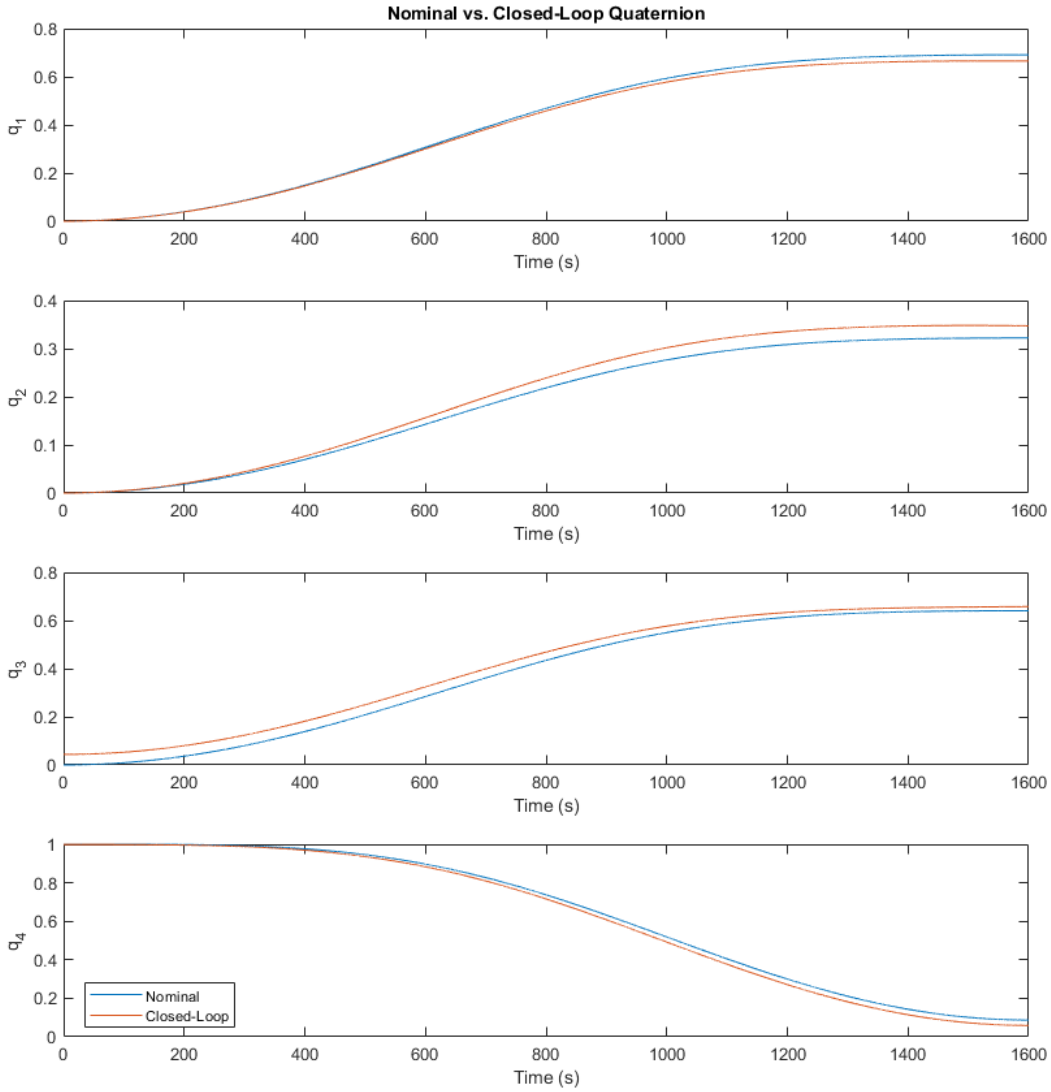

Figure 15: Quaternion

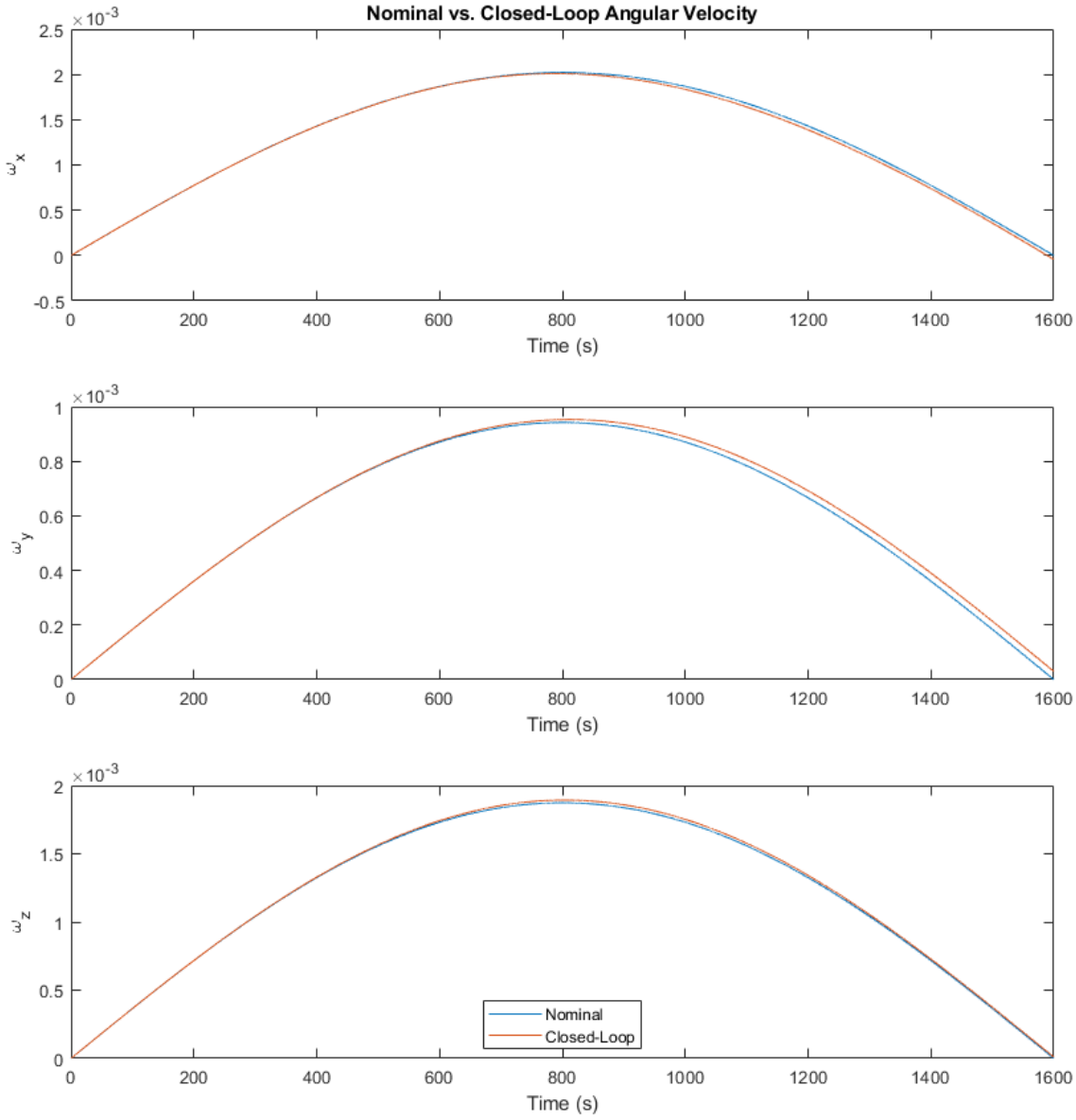

Figure 16: Angular Velocity

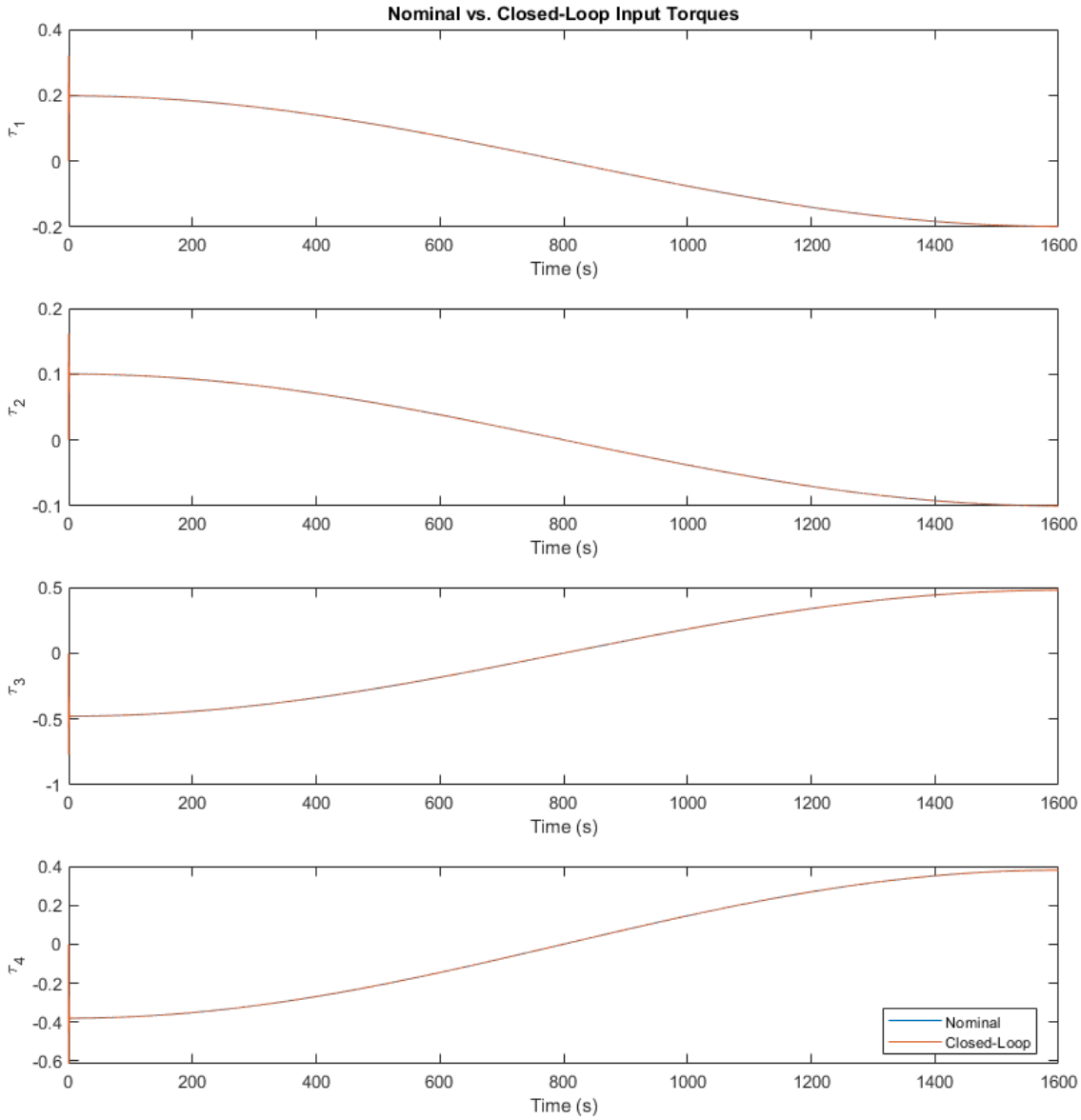

Figure 17: Input Torques

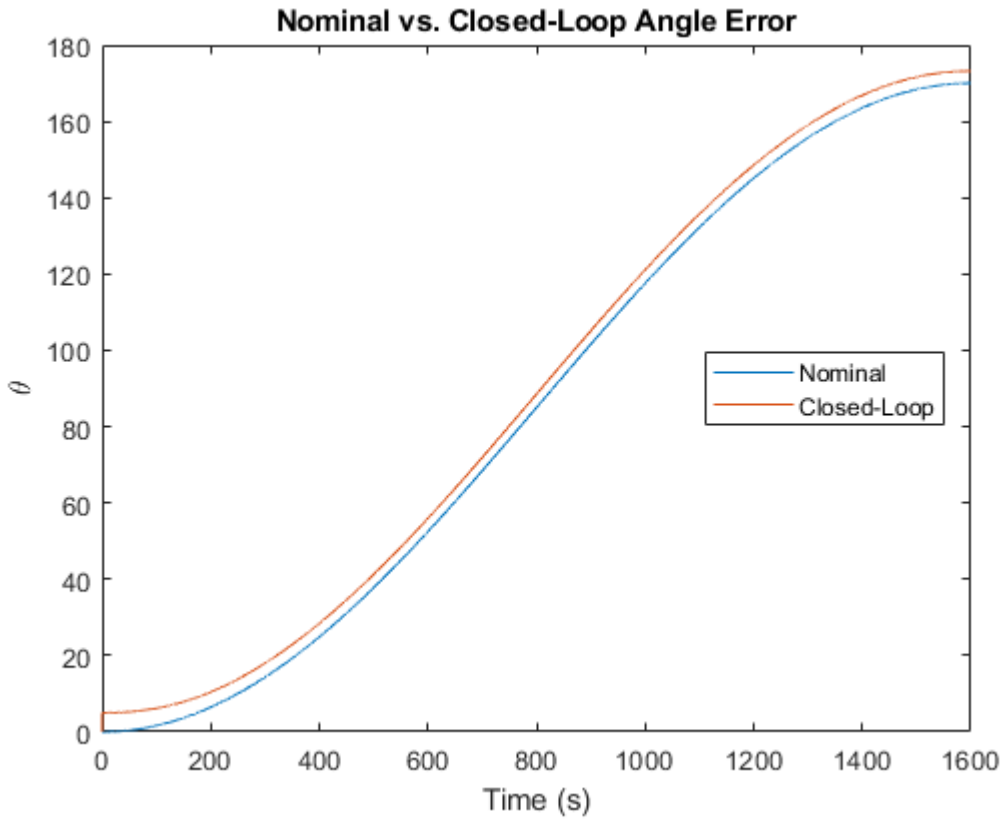

Figure 18: Axis-Angle Norm

5 HST Attitude Determination System

5.1 Sensor Specifications

The HST has five types of sensors that make up the Pointing Control System (PCS):

- Gyroscopes: Measures the telescope's 3-axis rotation rate in the satellite body frame. The gas-bearing gyros on the HST are arguably the most accurate and stable ever built. Limited hardware information is available for these gyros and for the sake of modeling bias and filtering, the following data is taken from more accessible gyros.
  - Rate Noise Density = 0.1 deg/s/$\sqrt{\text{Hz}}$.
  - Angular Random Walk = 0.1 deg/$\sqrt{\text{hr}}$.
- (Coarse) Sun Sensors: Determines the orientation of Hubble in relation to the Sun. The sensors use silicon diode detectors to determine whether the Sun is present in their field of view and the angle of the Sun relative to the sensor. This information is used to point the HST and protect the sensitive camera optics, which must be pointed at least 50^o away from the Sun at all times.
- Magnetometers: Measures the telescope's orientation in relation to Earth's magnetic field.
  - Magnetometer Error = 4 degrees
- Star Trackers: Determines the HST's attitude by measuring the location and brightness of stars in the sensor's field of view. This information is then compared to star almanacs to increase the accuracy of the HST's attitude when locking onto guide stars.
  - Star Tracker Error = 300 arcseconds
- Fine Guidance Sensors: Measures starlight captured by the telescope's mirrors to find and maintain a lock on guide stars to fix the satellite's attitude.
  - FGS Error = 2 milliarcseconds.

Noisy measurements can be simulated from the true quaternion dynamics by approximating error covariances from the accuracy of each sensor and treating the noise as a Gaussian white noise process.

5.2 Static State Estimation

Static attitude state estimation is performed by solving Wahba's Problem, the least squares cost function

$$L = \sum_{\lim_i} w_i \left\| {}^N r_i - {}^N Q^{BB} r_i \right\|_2^2$$

whose optimal solution represents the minimum rotation matrix Q between an inertial reference frame and the body frame of a satellite. There are many solution techniques for this optimization problem, and the following figure contains a summary of error results for a Monte Carlo simulation consisting of $N = 1500$ trials using the TRIAD algorithm, the Davenport q-method, and the SVD method. To simplify the static calculations, the algorithms use two body-frame measurements from the magnetometers. As expected, the Davenport method and the SVD method provided nearly identical results with approximately 5.24 degrees of error, which is less than the 5.70 degrees of error from the TRIAD algorithm. That being said, the error is significant using all three methods and a Kalman Filter must be implemented for better state estimation.

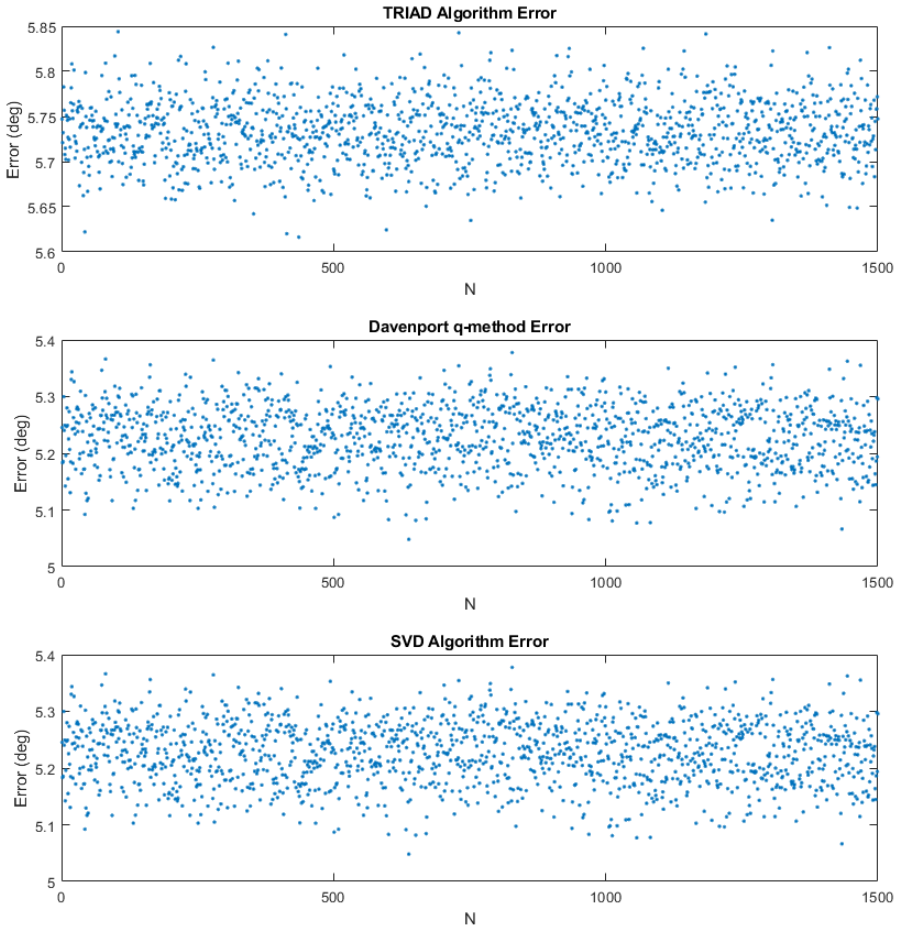

Figure 19: Monte Carlo Mean Error Results.

The following subplots represent the static attitude state estimates over a time span of 60 seconds. Over an averaged series of runs, the TRIAD algorithm required 0.5122 seconds to compute estimates over the entire time history. Interestingly, while the Davenport method and the SVD method provided identical estimates, the former method took only 0.2427 seconds whereas the latter method required 0.4886 seconds to compute estimates of the time history.

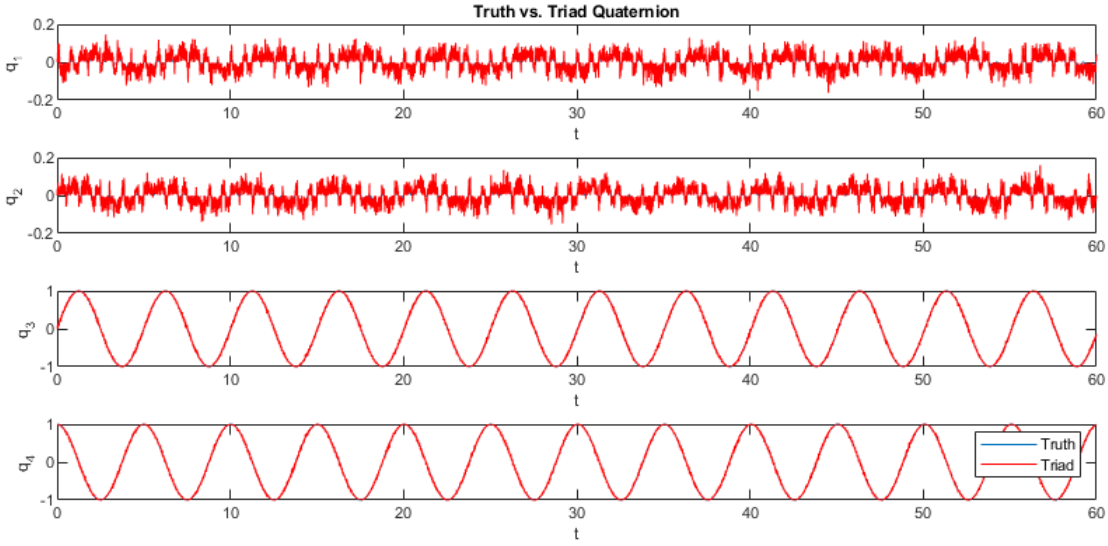

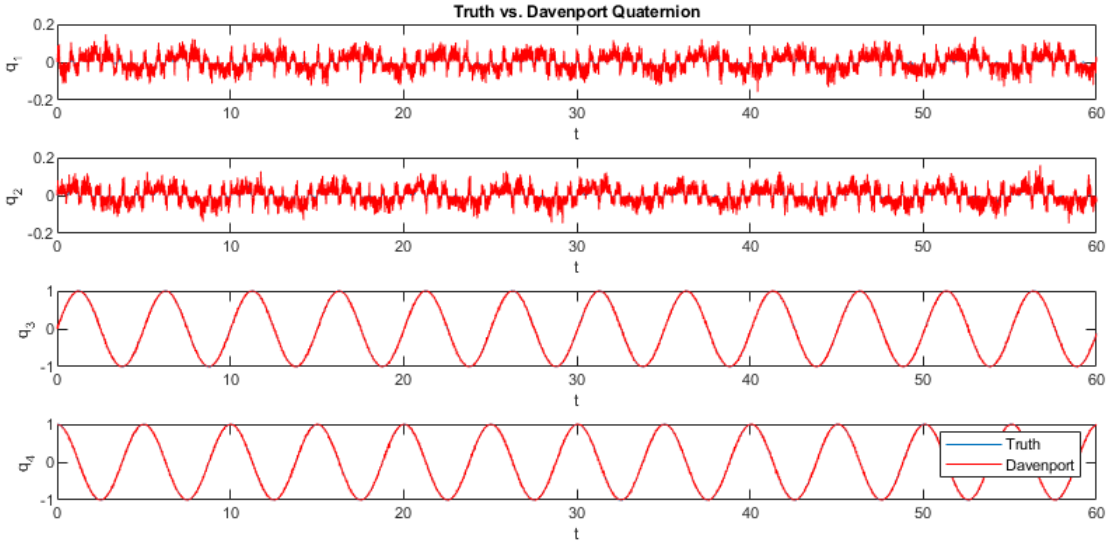

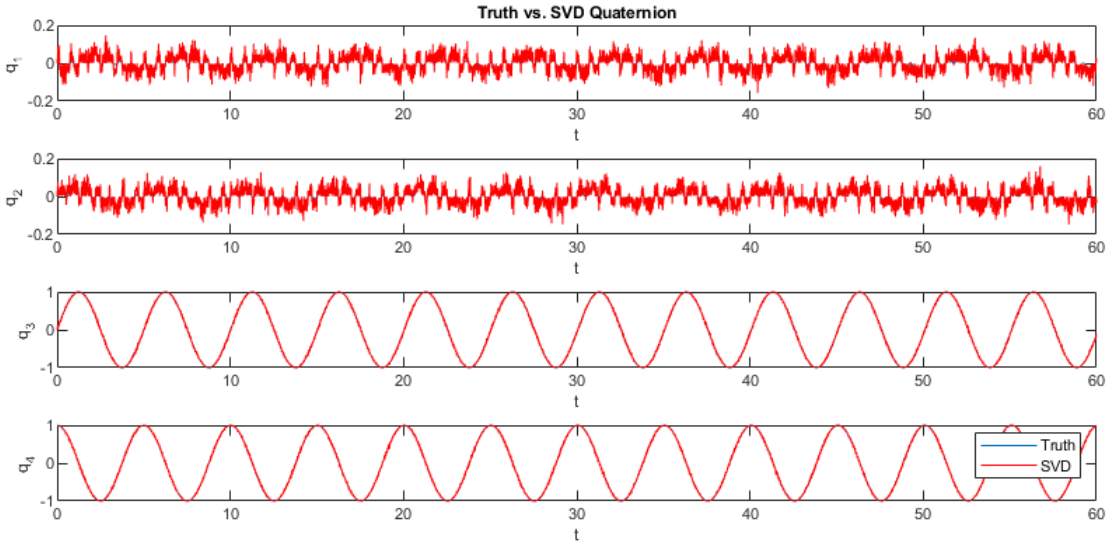
Truth vs. SVD Quaternion
q1
q2
q3
q4
t
Truth
SVD

5.3 Recursive Attitude Estimation

Using the simulated noisy measurements from the static state estimation, a Multiplicative Extended Kalman Filter can be implemented to recursively filter the sensor noise and estimate the satellite attitude and gyroscope bias with more accuracy than static methods. The process noise covariance $W \in \mathbb{R}^{6\times6}$ is chosen from specification data for the gyroscope and the sensor noise covariance $V \in \mathbb{R}^{9\times9}$ is selected based on error data from the sensor spec sheets. The MEKF fuses the measurements from the magnetometers, star tracker, and gyroscope, so we have

$$W = W_{gyro}, \qquad V = \begin{bmatrix} V_{st} & 0 & 0 \\ 0 & V_{mag} & 0 \\ 0 & 0 & V_{mag} \end{bmatrix}$$

where $W_{gyro} = (0.3046 \times 10^{-5})I_6$, $V_{st} = (0.2115 \times 10^{-5})I_3$, and $V_{mag} = (0.0049)I_3$. The MEKF estimates the state well within the two-sigma error bounds determined from the sensor covariances. The MEKF samples at 100 Hz, which is the same frequency at which the dynamics were simulated. Any substantial disparities between these two values produced suboptimal results, presumably due to signal aliasing. The tracking and error results are shown in the following figures for a 60 second simulation.

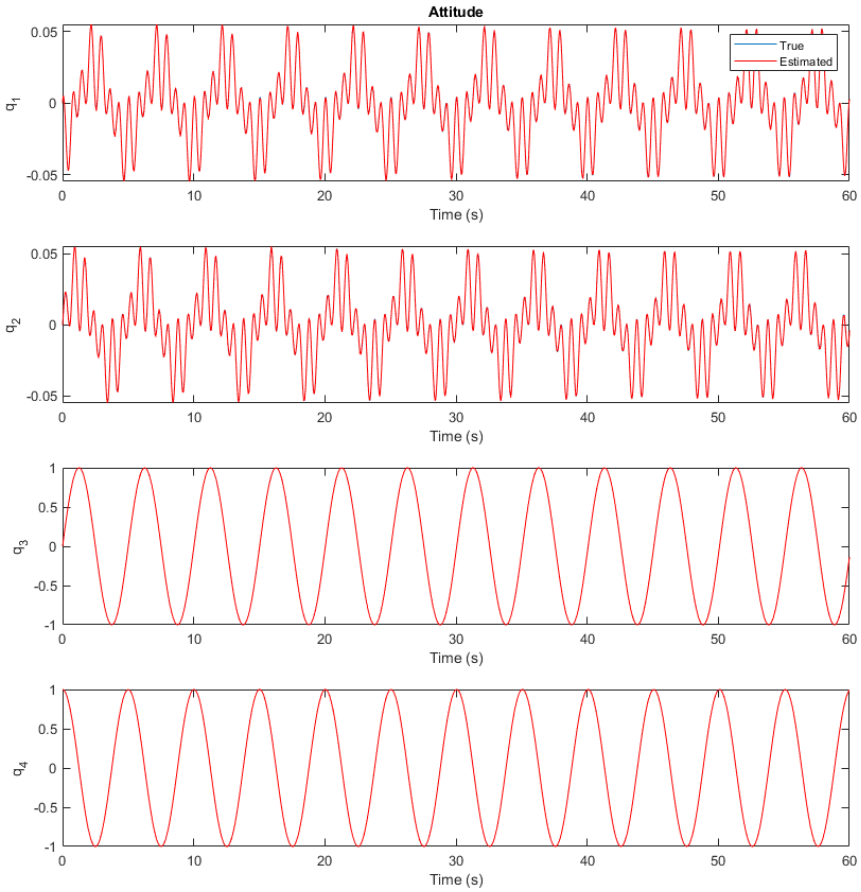

Figure 20: MEKF Attitude Estimate.

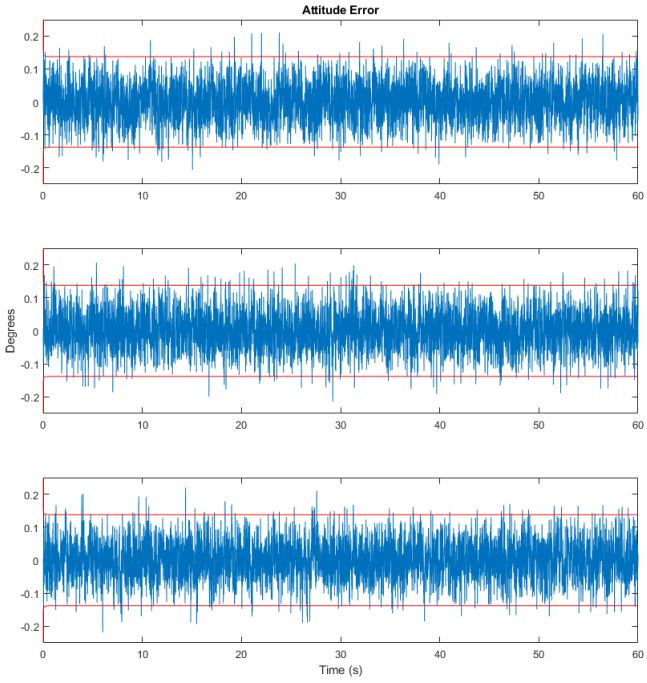

Figure 21: MEKF Attitude Estimate Error.

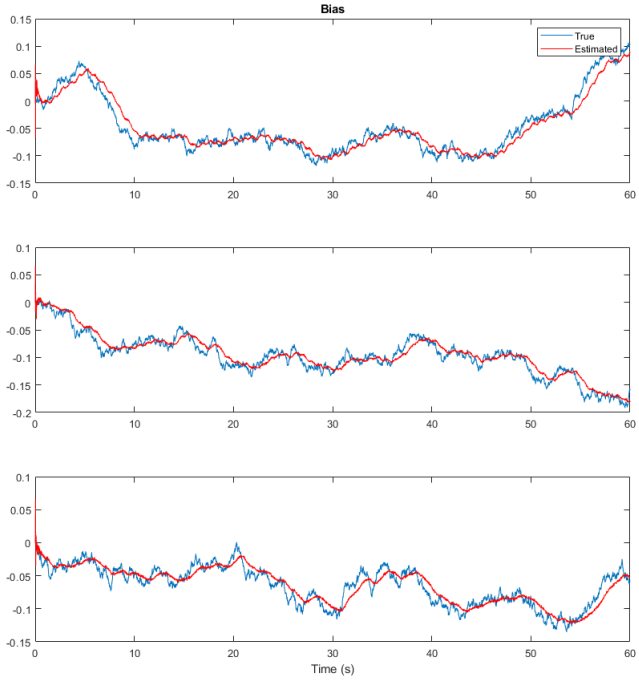

Figure 22: MEKF Bias Estimate.

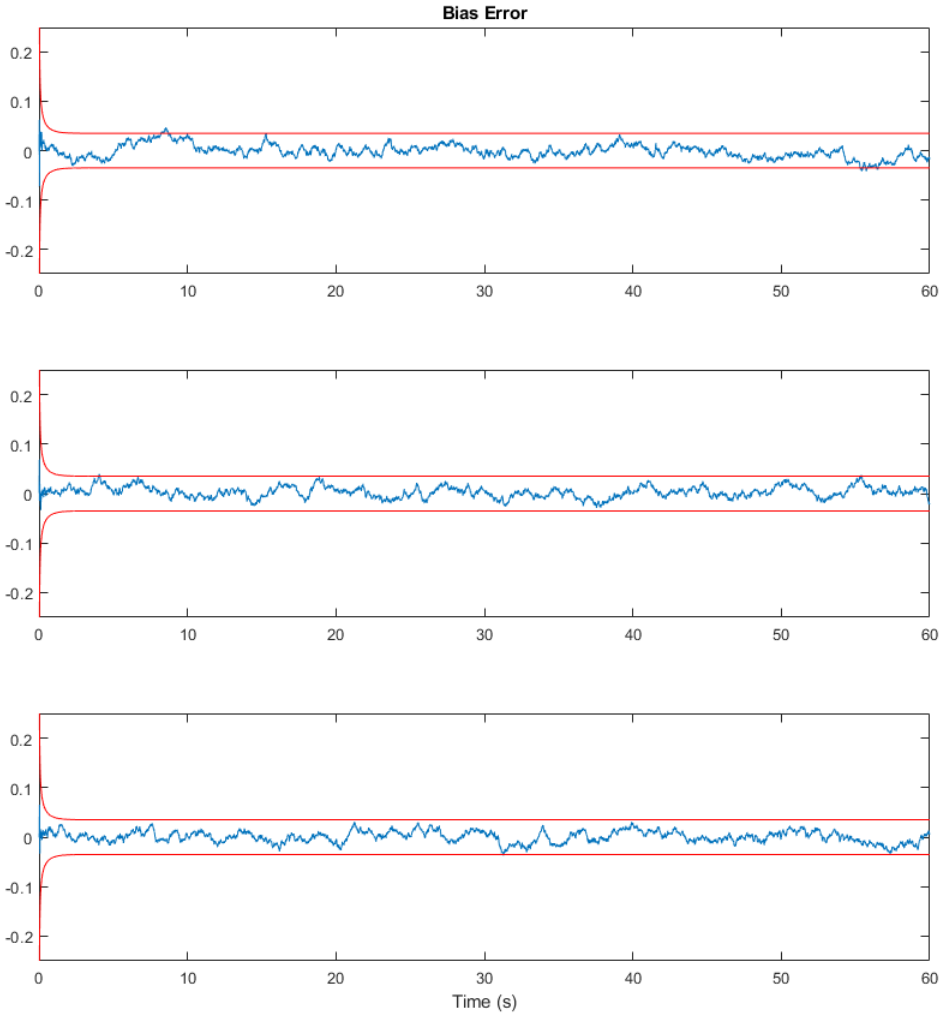

Figure 23: MEKF Bias Error.

6 Trajectory Optimization

6.1 Problem Setup

A time-optimal trajectory for a large-angle maneuver can be computed by representing the trajectory as a nonlinear program (NLP) and employing direct optimization methods such as multiple shooting and direct collocation. Choosing the latter method, the continuous time and dynamics are discretized into segments using N collocation or knot points. The control input for the discretized dynamics is applied as a zero-order hold (ZOH). For a minimum-time trajectory, the discrete cost function is the summation of the time steps, and the NLP setup is as follows:

$$\begin{aligned}
\min_{\bar{\mathbf{x}}} \quad & \sum_{k=1}^{N-1} \Delta t_k \\
\text{s.t.} \quad & x_{k+1} = x_k + a\left(\frac{x_k + x_{k+1}}{2}, u_k\right)\Delta t_k \\
& q_k^T q_k = 1 \\
& -u_{max} \leq u_k \leq u_{max} \\
& \Delta t_k = \Delta t_{k+1} \qquad \forall\, k \in \{0, ..., N-1\}
\end{aligned}$$

The decision variables for the attitude control problem are chosen to include the state, control, and time step at every knot point. For a spacecraft with reaction wheels, the full set of decision variables is

$$\bar{\mathbf{x}} = \left[\mathbf{q}_1,\ \omega_1,\ \rho_1,\ u_1,\ \Delta t_1,\ \ldots,\ \mathbf{q}_{N-1},\ \omega_{N-1},\ \rho_{N-1},\ u_{N-1},\ \Delta t_{N-1},\ \mathbf{q}_N,\ \omega_N,\ \rho_N,\right]^T$$

where the state is composed of the quaternion, angular velocity, and wheel momentum. The solution to the optimal control problem is subject to the dynamic constraints set by each knot point. Thus, the continuous dynamics are approximated by polynomial splines between knot points. For an acceptable balance between accuracy and computation cost, midpoint collocation is used for this problem. With this approach, the dynamics between two knot points are approximated as a line with the slope equal to the slope at the midpoint

$$x_{k+1} = x_k + f(\frac{x_{k+1} + x_k}{2}, u_k)\Delta t_k$$

where $f(x_k, u_k)$ represents the dynamics of the system such that

$$\dot{x}(t) = f(x(t), u(t))$$

The first dynamic equation is that of the quaternion kinematics

$$\dot{\mathbf{q}} = \frac{1}{2}\mathbf{q}\begin{bmatrix}\omega \\ 0\end{bmatrix}$$

The second equation is given by the gyrostat equation

$$\begin{aligned}
& J\dot{\omega} + \dot{\rho} + \omega \times (J\omega + \rho) = \tau = 0 \\
\implies & \dot{\omega} = -J^{-1}(\dot{\rho} + \omega \times (J\omega + \rho))
\end{aligned}$$

Where J is the inertia tensor, and τ is an external torque. For this system, it is assumed that there are no external torques and the control input is a torque generated from the reaction wheels. Because the wheel momentum is incorporated into the state dynamics, the third equation is simply

$$\dot{\rho} = u$$

An unfortunate disadvantage of collocation methods is that the formulated NLP is quite large. For this problem, the solver must optimize over $14N$ states, subject to approximately $12N$ decision variable constraints. Furthermore, for maneuvers that occur over a long period of time such as those done with reaction wheels, it is necessary to interpolate the continuous dynamics to obtain a manageable number of knot points. Two main strategies for speeding up the solver include manually inputting the gradient of the objective function and the constraint equations and priming the solver with a feasible solution. Without the gradients, the solver would use an approach such as finite differencing to approximate the gradients, which would slow the solver significantly. To ensure that the solver converged to a feasible solution, a time history of states and controls from the eigen-axis slew was provided as a "baseline" for the solver. In general, a global optimum will not be found because the problem is not convex.

6.2 Results

The optimal control problem is solved using Interior Point Optimizer (IPOPT), with SQP as the solution algorithm. The results are shown in the following figures for a 180^o maneuver and $N = 101$ knot points.

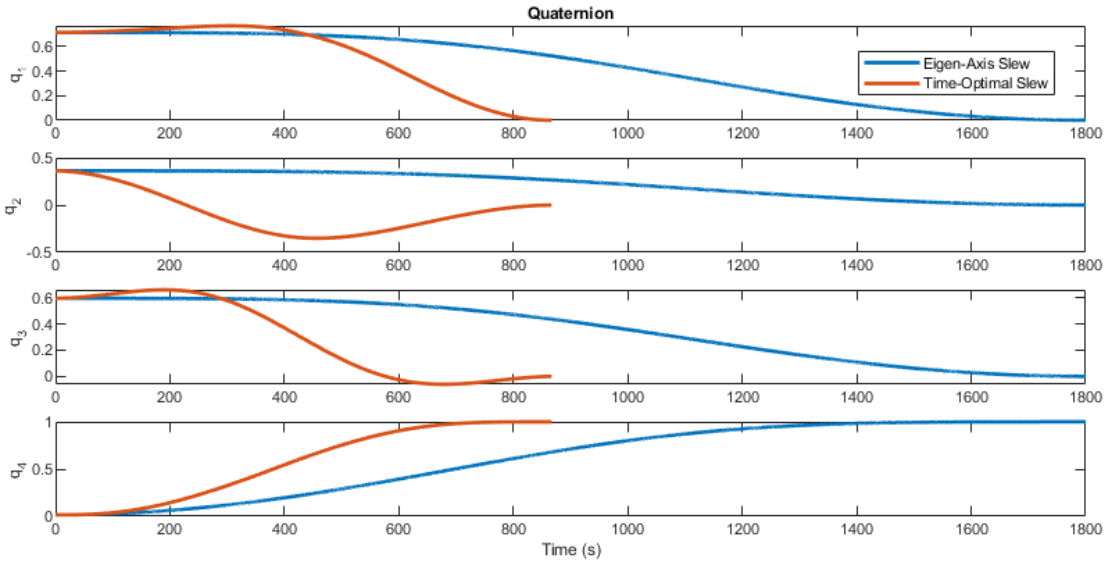

Figure 24: Time-Optimal Quaternion.

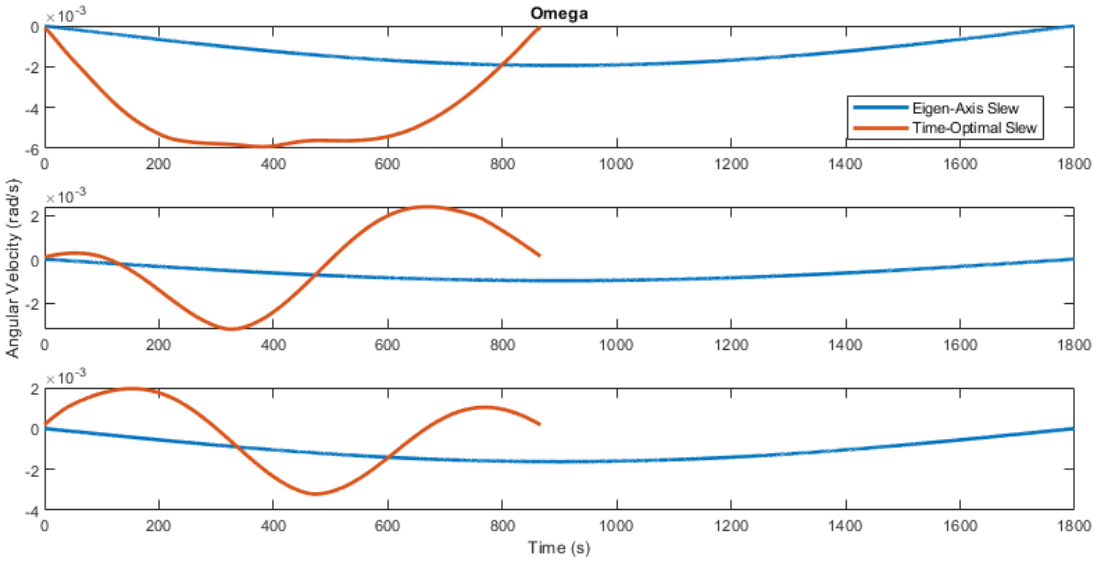

Figure 25: Time-Optimal Angular Velocity.

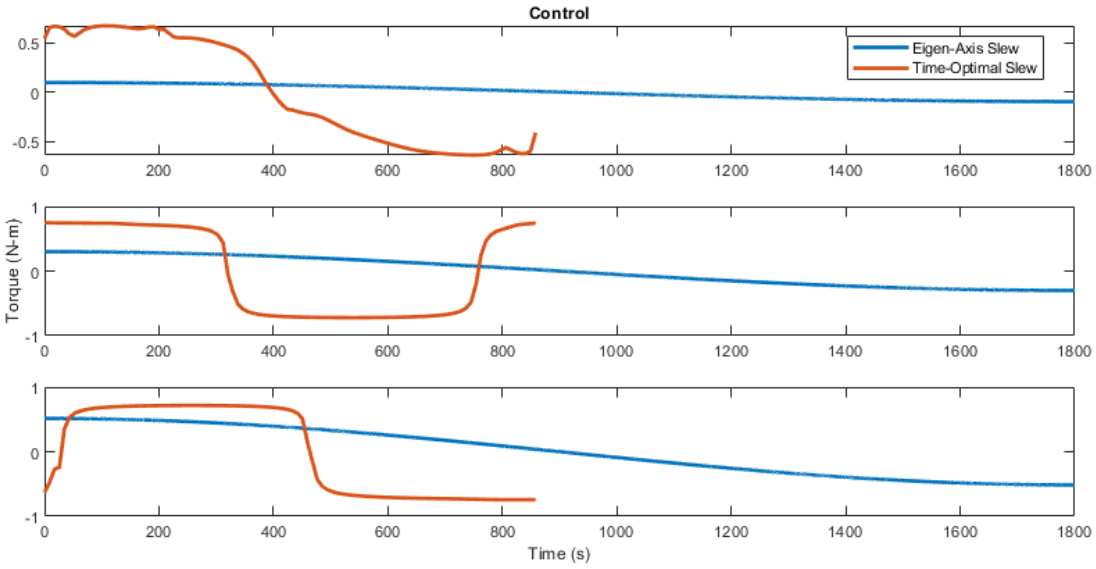

Figure 26: Time-Optimal Control.

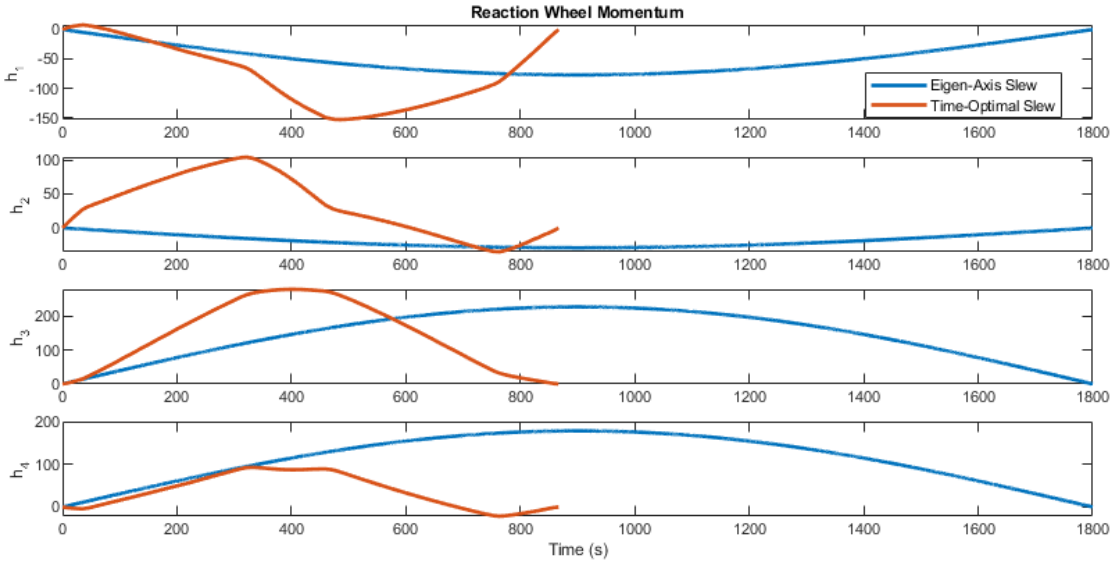

Figure 27: Time-Optimal Reaction Wheel Momentum.

The reference eigen-axis slew takes place over 1800 seconds, whereas the maneuver with time-optimal control is completed in 866 seconds. The solver required 16 minutes to converge to a solution. It is evident from the figures that the optimal maneuver takes advantage of its inertial properties and actuation capabilities in all three axes to produce a substantial time improvement. As desired, the optimal solution obeys the torque limit $\tau_i = 0.8$ N-m and angular momentum limit $h_j = 350$ kg-m^2/s of the reaction wheels over the entire trajectory. In at least two axes, the solution resembles a bang-bang control scheme similar to most time-optimal problems. Extensions of this problem include the use of higher-order collocation methods and the investigation of more complicated control architectures such as underactuation with reaction wheels or magnetorquers. Another option is the incorporation of "forbidden" pointing regions as constraints for satellites with sensitive on-board optics.

References

[1] Hubble Space Telescope Fact Sheet. Retrieved April 24, 2018, from http://www.spacetelescope.org/about/general/fact_sheet/

[2] Hubble Space Telescope Primer for Cycle 25. Retrieved April 24, 2018, from http://www.stsci.edu/hst/proposing/documents/primer/primer.pdf

[3] The Telescope: Hubble Essentials. Retrieved April 24, 2018, from http://hubblesite.org/the_telescope/hubble_essentials/

[4] About the Hubble Space Telescope. Retrieved April 24, 2018, from https://www.nasa.gov/mission_pages/hubble/story/index.html

[5] Hubble Space Telescope Pointing Control System. Retrieved April 24, 2018, from https://www.nasa.gov/content/goddard/hubble-space-telescope-pointing-control-system

[6] Hubble Space Telescope. Retrieved April 24, 2018, from https://en.wikipedia.org/wiki/Hubble_Space_Telescope

[7] Alfriend, K., Vadali S., Gurfil P., How J., Breger L. (2010). *Spacecraft Formation Flying: Dynamics, Control, and Navigation*. Elsevier Astrodynamics Series.

[8] Olivares, A., Staffetti, E. (2018). Time-Optimal Attitude Scheduling of a Spacecraft Equipped with Reaction Wheels. *International Journal of Aerospace Engineering, 2018,* 1-14.

[9] Lee, U., Mesbahi, M. (2014). Quaternion-Based Optimal Spacecraft Reorientation Under Complex Attitude Constrained Zones. *Advances in the Astronautical Sciences, 150,* 1995-2010.

[10] Bingqian, J., Dong, Y., Zhaowei, S. (2014). Trajectory Optimization for Satellite Fast Attitude Maneuver Based on Collocation Method. *International Conference on Mechatronics and Control.*

[11] Betts, J.T. (1998). Survey of Numerical Methods for Trajectory Optimization. *Journal of Guidance, Control, and Dynamics, 21*(2), 193-207.

[12] Bilimoria, K. D., & Wie, B. (1993). Time-Optimal Three-Axis Reorientation of a Rigid Spacecraft. *Journal of Guidance, Control, and Dynamics, 16*(3), 446-452.

[13] Crassidis, J.L., & Markley, F.L. (2014). *Fundamentals of Spacecraft Attitude Determination and Control.* New York, NY: Springer-Verlag.